Electromechanical behavior of [001]-textured Pb(Mg1/3Nb2/3)O3-PbTiO3 ceramics

Yongke Yan, Yu. U. Wang, and Shashank Priya

Citation: Applied Physics Letters **100**, 192905 (2012); doi: 10.1063/1.4712563
View online: http://dx.doi.org/10.1063/1.4712563
View Table of Contents: http://scitation.aip.org/content/aip/journal/apl/100/19?ver=pdfcov
Published by the AIP Publishing

Electromechanical behavior of [001]-textured $Pb(Mg_{1/3}Nb_{2/3})O_3$-$PbTiO_3$ ceramics

Yongke Yan,[1] Yu. U. Wang,[2] and Shashank Priya[1,a)]
[1]*Bio-Inspired Materials and Devices Laboratory (BMDL), Center for Energy Harvesting Materials and Systems (CEHMS), Virginia Tech, Blacksburg, Virginia 24061, USA*
[2]*Department of Materials Science and Engineering, Michigan Tech, Houghton, Michigan 49931, USA*

(Received 21 January 2012; accepted 21 April 2012; published online 8 May 2012)

[001]-textured $Pb(Mg_{1/3}Nb_{2/3})O_3$-$PbTiO_3$ (PMN-PT) ceramics were synthesized by using templated grain growth method. Significantly high [001] texture degree corresponding to 0.98 Lotgering factor was achieved at 1 vol. % $BaTiO_3$ template. Electromechanical properties for [001]-textured PMN-PT ceramics with 1 vol. % $BaTiO_3$ were found to be $d_{33} = 1000$ pC/N, $d_{31} = 371$ pC/N, $\varepsilon_r = 2591$, and $\tan\delta = \sim 0.6\%$. Elastoelectric composite based modeling results showed that higher volume fraction of template reduces the overall dielectric constant and thus has adverse effect on the piezoelectric response. Clamping effect was modeled by deriving the changes in free energy as a function of applied electric field and microstructural boundary condition. © *2012 American Institute of Physics*. [http://dx.doi.org/10.1063/1.4712563]

Templated grain growth (TGG) has proven to be a cost effective process for fabricating crystallographically oriented high performance piezoelectric ceramics,[1–3] such as lead-free $(Bi_{1-x}Na_x)TiO_3$ (BNT) based,[4] $(K_{1-x}Na_x)NbO_3$ (KNN) based,[5] and lead-based $Pb(Mg_{1/3}Nb_{2/3})O_3$-$PbTiO_3$ (PMN-PT) (Refs. 2, 3, and 6–8) compositions. For texturing PMN-PT ceramic, perovskite $BaTiO_3$ (BT) and $SrTiO_3$ (ST) which have same crystallographic structure with similar lattice parameters and can be synthesized into well-faceted high-aspect ratio crystallites have been chosen as substitution.[2,3,6] However, heterogeneous templates inevitably degrade the performance of sintered ceramic mainly because of interfacial diffusion and stress clamping between matrix and templates.[2,3] For example, dissolution of ST template in PMN-PT results in an unacceptably low depolarization temperature (~60 °C).[3] BT template is stable in PMN-PT, but residual templates reduce the strain response of textured ceramics via mechanical clamping.[2] To reduce the adverse effect of heterogeneous template on the property of textured ceramics, it is important to reduce the concentration of heterogeneous template. In previous studies,[2,3,9] normally, 5 vol. % template was added to achieve >90% texture degree and enhancement in the piezoelectric properties. In this letter, we quantify the effect of BT template concentration on the texture degree and resulting changes in properties of PMN-PT and show that even 1 vol. % template can provide >90% texture degree. Next, we model the response of the textured ceramics by deriving the change in free energy as a function of applied electric field and microstructural inhomogeneity. The model clearly revealed the effect of composite structure and clamping, validating the experimental results.

$0.675Pb(Mg_{1/3}Nb_{2/3})O_3$-$0.325PbTiO_3$ ceramics were textured by TGG process using x vol. % of $BaTiO_3$ template, abbreviated as PMN-PT-xBT ($x = 0$, 0.5, 1, 3, 5). The TGG process and synthesis of BT template have been described in detail elsewhere.[6] The texture degree was calculated from x-ray diffraction data (XRD, PANalytical X'Pert) by Lotgering factor method.[10] The microstructure was observed by using scanning electron microscopy (SEM, FEI Quanta 600 FEG). The relative permittivity (ε_r) and loss ($\tan\delta$) were measured by using a multi-frequency Inductance-Capacitance-Resistance (LCR) meter (HP4287A). Electromechanical coupling factor was obtained by impedance/gain analyzer (HP4194A). The piezoelectric coefficient d_{33} was measured by using YE 2730 A d_{33}-meter (APC Products, Inc.). The polarization vs. electric field hysteresis curves were measured by using a modified Sawyer-Tower circuit (Precision Premier II).

Figure 1(a) shows the XRD patterns of PMN-PT-xBT sintered specimens. All patterns display pervoskite structure without any noticable secondary phase. With the introduction of templates, intensities of (00l) peaks increase rapidly while other peaks show significantly reduced intensity, indicating the formation of texture. Figure 1(b) shows the texture degree computed by Lotgering factor method as a function of BT concentration. PMN-PT-0BT represents the random polycrystalline ceramics. With increase of BT template content, the texture degree increases dramatically and then saturates for PMN-PT-1BT. Figure 1(c) displays the cross-sectional SEM image of PMN-PT-1BT specimen. It shows brick wall-like structure. BT templates (black lines) were well aligned in the matrix, and there were almost no residual random-oriented matrix grains contrary to PMN-PT-0BT as shown in Fig. 1(d). This microstructure is consistent with the high texture degree as indicated by XRD. These results clearly show that PMN-PT-1BT with 1 vol. % template was almost fully textured ($f = 0.98$). This is a significant achievement with important implications towards application of piezoelectric ceramics. We found that optimum dimension for BT template microcrystals to achieve high texture degree was in the vicinity of length: $5 \sim 10\ \mu$m and thickness: $0.5 \sim 1\ \mu$m. At these dimensions, the required growth distance for inducing texture in the matrix is dramatically reduced on the order of ~3–7 μm.

Figure 2(a) shows the piezoelectric coefficient (d_{33}) and dielectric loss ($\tan\delta$) of PMN-PT-xBT specimen. With increase of BT content, the d_{33} increases dramatically and

a)Electronic mail: spriya@vt.edu.

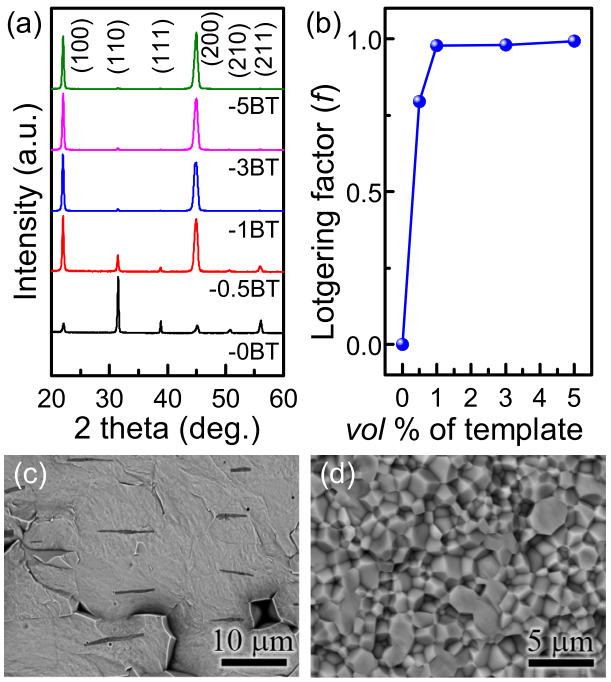

FIG. 1. (a) XRD patterns of PMN-PT-xBT ceramics; (b) texture degree of PMN-PT ceramics as a function of BT concentration; cross-sectional SEM images of (c) PMN-PT-1BT and (d) PMN-PT-0BT ceramic.

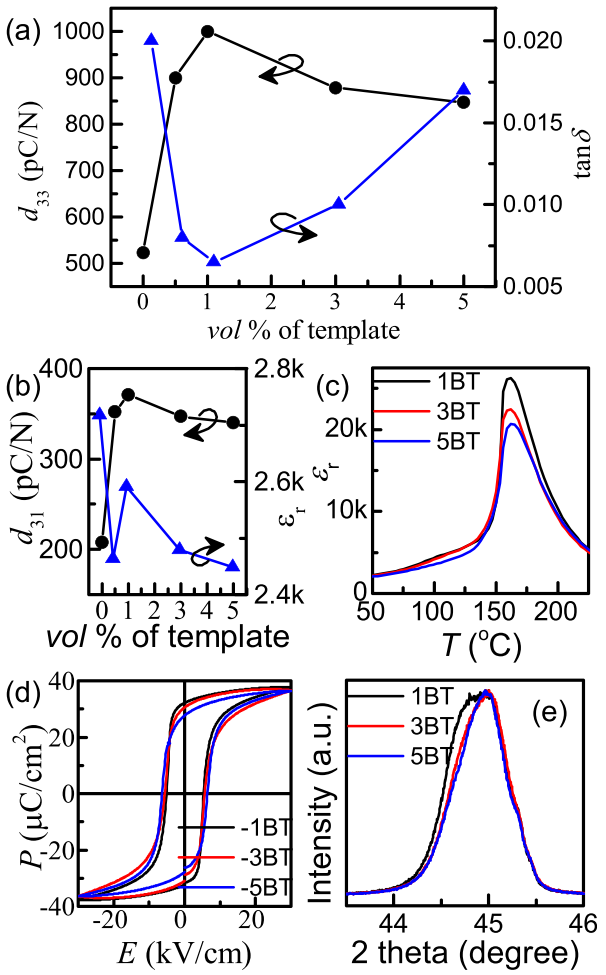

FIG. 2. (a,b) Dielectric and piezoelectric properties of PMN-PT-xBT ceramics; (c) Dielectric permittivity as a function of temperature for PMN-PT-xBT ceramics; (d) Polarization (P) vs. electric field, (E) hysteresis loops; and (e) XRD patterns of PMN-PT-xBT ceramics.

achieves the maximum value of 1000 pC/N at $x = 1$, corresponding to the texture development as shown in Fig. 1(b). In this range ($0 \leq x \leq 1$), the enhancement of piezoelectric response is attributed to the texture engineering which develops domain configurations similar to that in the single crystal. Further increasing the BT content, the d_{33} gradually decreases. Similar trend can also be observed in the change of d_{31} as shown in Fig. 2(b). On the other hand, variation in tanδ is contrary to that for d_{33}. The lowest value of tanδ ($\sim$0.6%) was achieved for PMN-PT-1BT ceramic, which is about 1/3rd of the magnitude obtained for most of the soft piezoelectric ceramics (>2.0%). High piezoelectric response with low loss makes PMN-PT-1BT system an ideal substitute for currently deployed soft piezoelectrics.

In spite of increasing degree of texture, decrease in d_{33} for x > 1 samples can be understood by considering Eq. (1), relating piezoelectric coefficient d_{33} with electrostrictive constant Q_{11}, relative permittivity (ε_r), and remnant polarization (P_r),

$$d_{33} = 2Q_{11}\varepsilon_0\varepsilon_r P_r. \quad (1)$$

Since relative permittivity for the poled PMN-PT-xBT at room temperature decreases with x for $x > 1$ (Fig. 2(b)), it can account for decrease in d_{33} values. Same tendency of maximum relative permittivity for unpoled PMN-PT-xBT can be found in the Fig. 2(c). It should be noted here that no obvious T_c shift in PMN-PT-xBT specimen indicates BT is very stable in PMN-PT ceramics, which is different from $SrTiO_3$ textured PMN-PT ceramic.[1] Therefore, the decrease of ε_r may be associated with the elastoelectric composite effect due to the introduction of low permittivity BT template ($\varepsilon_r = 130$ in $\langle 001 \rangle$ direction). Figure 2(d) shows the polarization (P) vs. electric field (E) for the PMN-PT-xBT specimen in the range of $x > 1$. It can be seen that P_r decreases and coercive field (E_c) increases with increasing BT template content (x), which indicates that the domain motion and switching became more difficult. This phenomenon may be attributed to clamping effect of BT template. The stress comes from the lattice mismatch between BT template and PMN-PT matrix and also from their large difference in electromechanical properties. Sabolsky has shown that this stress is high enough to depole the textured PMN-PT ceramic at large dimensions ($\sim$100 μm) of BT template.[2] The stress build-up also results in phase shift from rhombohedral side to tetragonal side.[2] In our study, fine BT template crystals were used which reduces the magnitude of stress. Even then, as shown in Fig. 2(e), the width of (002) peaks decreases indicating phase shift from morphotropic phase boundary (MPB) (coexistence of rhombohedral and tetragonal phase) to tetragonal side. Therefore, elastoelectric composite effect and clamping effect can be suggested to degrade the piezoelectric property when texture degree saturates.

Textured PMN-PT ceramics can be considered as a composite consisting of matrix PMN-PT and BT templates as shown in Fig. 3(a). In ideal condition, the required growth distance (x) of PMN–PT crystal on BT template for 100% texture degree can be calculated by the following equation:

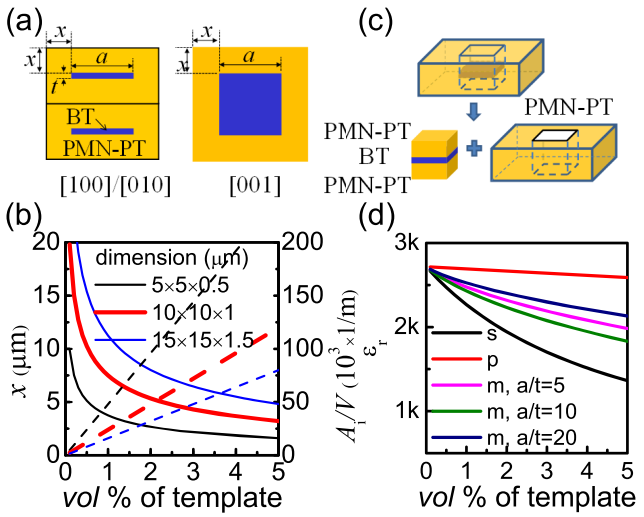

FIG. 3. (a) Schematic illustration of grains of textured ceramic. (b) Required growth distance (x) of matrix (solid line) and specific interface area (A_i/V) (dashed line) as a function of the volume fraction and dimensions of template. (c) Schematic illustration of single templated grain. (d) Calculated relative permittivity of fully textured PMN-PT ceramic as a function of the volume fraction and dimensions of BT template.

$$\frac{a^2 t}{V_T} = (2x + a)^2 (2x + t), \tag{2}$$

where a is the dimension of template plane, t is the thickness of template, and V_T is the volume fraction of template. Figure 3(b) shows the variation of x as a function of the volume fraction and dimensions of template. Higher the template content shorter the growth distance, thus, it is easier to achieve full texture. As shown in Fig. 3(c), this composite can be considered as both parallel and series connections between PMN-PT matrix and BT template. In these two cases, effective permittivity of composite can be given by Eqs. (3) and (4), respectively,

$$\varepsilon_{parallel} = \varepsilon_t V_T + \varepsilon_m (1 - V_T), \tag{3}$$

$$\varepsilon_{serial} = \left[\frac{\varepsilon_t \varepsilon_m}{\varepsilon_m V_T + \varepsilon_t (1 - V_T)} \right], \tag{4}$$

where ε_m and ε_t are the relative permittivity of PMN-PT matrix and BT template, respectively. Since the textured sample is composed of both parallel and serial connection between PMN-PT matrix and BT templates (Fig. 3(c)), the relative permittivity of this composite structure (ε_{mixed}) was calculated by the following expression:

$$\varepsilon_{mixed} = \left[\frac{\varepsilon_m \frac{4x^2 + 4ax}{2x + t} + \frac{a^2 \varepsilon_t \varepsilon_m}{2x\varepsilon_m + t\varepsilon_t}}{\frac{(2x + a)^2}{2x + t}} \right]. \tag{5}$$

Figure 3(d) shows the theoretical relative permittivity for 100% textured ceramics as a function of the volume fraction and dimensions of template. Here, the relative permittivity is calculated from Eqs. (3)–(5) by using $\varepsilon_m = 2718$ for PMN-PT matrix grains and $\varepsilon_t = 130$ for $\langle 001 \rangle$ BT template.[11]

As shown in Fig. 3(b), the specific interface area (A_i/V) related to clamping effect increases linearly with the BT template content. To further clarify the clamping effects of BT template content, texture degree, and material property mismatches between PMN-PT and BT on the dielectric and piezoelectric properties of the textured PMN-PT ceramics, we modeled the electrical behavior of the system by accounting the microstructural boundary conditions. The total free energy F of matrix-template composite system under externally applied electric field $\mathbf{E}^{ex}$ is given as[12,13]

$$F = \int d^3 r \left[\frac{P^2(\mathbf{r})}{2\varepsilon_0 \chi(\mathbf{r})} - E_k^{ex} P_k(\mathbf{r}) \right] + \frac{1}{2} \int \frac{d^3 k}{(2\pi)^3} \left[\frac{n_i n_j}{\varepsilon_0} \tilde{P}_i \tilde{P}_j^* + K_{ijkl} \tilde{\varepsilon}_{ij} \tilde{\varepsilon}_{kl}^* \right], \tag{6}$$

where ε_0 is the permittivity of free space, $\chi(\mathbf{r})$ is the phase-dependent dielectric susceptibility that describes the composite microstructure, $\tilde{\mathbf{P}}(\mathbf{k})$ is the Fourier transform of the polarization field $\mathbf{P}(\mathbf{r})$, $\mathbf{n} = \mathbf{k}/k$ is a unit directional vector in $\mathbf{k}$-space, K_{ijkl} combines elastic constants and serves as an effective elastic stiffness tensor, and $\tilde{\varepsilon}(\mathbf{k})$ is the Fourier transform of the electrostrictive strain field $\varepsilon(\mathbf{r})$. The $\mathbf{r}$-space integral in Eq. (6) describes the dielectric response of individual phases in the composite under electric field, and the $\mathbf{k}$-space integral describes the electrostatic and elastic energies, respectively, due to inhomogeneous polarization distribution in the composite and mechanical clamping between the matrix and templates. While Eq. (6) can be numerically solved to perform large-scale computer simulation studies,[12,13] it can be analytically simplified in the case of the textured PMN-PT ceramics based on the specific microstructure morphology as observed from the SEM image of Fig. 1(c): BT platelet templates exhibit high aspect ratio ($\rho = a/t \sim 10$), are well dispersed in the matrix with large separation distance at low volume fraction ($V_T < 5\%$), and are aligned parallel to tape plane via tape casting. In such a situation, the $\mathbf{k}$-space integrals in Eq. (6) can be analytically integrated for platelets,[14] and the energy density (per unit volume) of the composite under external electric field applied normal to the template platelets becomes

$$\begin{aligned} F(P_T, P_{M'}, P_{M''}, E^{ex}) = {} & V_T \frac{P_T^2}{2\varepsilon_0 \chi_T} + V_{M'} \frac{P_{M'}^2}{2\varepsilon_0 \chi_M} + V_{M''} \frac{P_{M''}^2}{2\varepsilon_0 \chi_M} \\ & + \frac{V_T V_{M'}}{V_T + V_{M'}} \frac{(P_T - P_{M'})^2}{2\varepsilon_0 \chi_0} \\ & + \frac{V_T V_{M'}}{V_T + V_{M'}} \frac{Y[b_{31}^T P_T - b_{31}^M P_{M'}]^2}{1 - \nu} \\ & - (V_T P_T + V_{M'} P_{M'} + V_{M''} P_{M''}) E^{ex}. \end{aligned} \tag{7}$$

In arriving at Eq. (7), the composite volume is approximately separated into three parts of volume fractions V_T, $V_{M'}$, and $V_{M''}$, respectively, where V_T is BT template volume fraction, $V_{M'} \approx \rho V_T$ is the volume fraction of PMN-PT matrix that is in parallel connection with BT platelets, thus is both mechanically clamped by the templates and electrostatically affected by the matrix-template interfacial charges, and $V_{M''}$ ($= 1 - V_T - V_{M'}$) is the volume fraction of the rest PMN-PT matrix that is not affected by mechanical clamping or interfacial charges. Thus, Eq. (7) takes into account the mixed nature of both parallel and serial connections between

PMN-PT matrix and BT templates in the composite. It is worth noting that the volume $V_{M'} \approx \rho V_T$ is approximated using the template aspect ratio ρ (~10) in accordance with Saint-Venant's principle[15] that states internal fields diminish with distance comparable to heterogeneity dimensions, allowing simplification of the internal boundary conditions and analytical evaluation of the electrostatic and elastic energies in a template-matrix volume $(V_T + V_{M'})$ around the thin platelet inclusions.[14] It must be noted that the result in Eq. (7) is valid only for composites of well dispersed platelet templates at low volume fraction (i.e., $V_T < 5\%$) and under external electric field applied normal to the template platelets (i.e., along tape thickness direction), as is the case here. In Eq. (7), P_T, $P_{M'}$, and $P_{M''}$ are the polarizations induced by the external field $\mathbf{E}^{ex}$ in three respective volume parts, χ_T, χ_M and b_{31}^T, b_{31}^M are the dielectric susceptibilities and piezoelectric polarization coefficients of BT template and PMN-PT matrix, respectively, χ_0 is a background dielectric susceptibility attenuating electrostatic interactions, and Y and ν are Young's modulus and Poisson's ratio, respectively. To predict the dielectric and piezoelectric responses of the composite, the values of P_T, $P_{M'}$, and $P_{M''}$ are first obtained for nonzero field $\mathbf{E}^{ex}$ by solving,

$$\frac{\partial F}{\partial P_T} = 0, \qquad \frac{\partial F}{\partial P_{M'}} = 0, \qquad \frac{\partial F}{\partial P_{M''}} = 0. \tag{8}$$

The dielectric susceptibility χ and piezoelectric strain coefficients d_{33} and d_{31} of the composite are then determined from the obtained P_T, $P_{M'}$, and $P_{M''}$ according to expressions,

$$\chi = \frac{V_T P_T + V_{M'} P_{M'} + V_{M''} P_{M''}}{\varepsilon_0 E^{ex}}, \tag{9}$$

$$d_{33} = \frac{V_T b_{33}^T P_T + V_{M'} b_{33}^M P_{M'} + V_{M''} b_{33}^M P_{M''}}{E^{ex}}, \tag{10}$$

$$d_{31} = \frac{V_T b_{31}^T P_T + V_{M'} b_{31}^M P_{M'} + V_{M''} b_{31}^M P_{M''}}{E^{ex}}. \tag{11}$$

For calculations, the following material parameters were used:[11,16] $\chi_T = 130$, $\chi_M = 2718$, $d_{31}^T = -33 \times 10^{-12}$ C/N, $d_{33}^T = 90 \times 10^{-12}$ C/N, $d_{31}^{MR} = -210 \times 10^{-12}$ C/N, $d_{31}^{MT} = -400 \times 10^{-12}$ C/N, $d_{33}^{MR} = 520 \times 10^{-12}$ C/N, $d_{33}^{MT} = 1000 \times 10^{-12}$ C/N, $\chi_0 = 1000$, $Y = 100 \times 10^9$ N/m^2, and $\nu = 0.3$, where the superscripts MR and MT indicate random (non-textured) and fully [001]-textured PMN-PT matrix, respectively. The piezoelectric polarization b-coefficients are obtained from the piezoelectric strain d-coefficients from the relation $b = (\varepsilon_0 \chi)^{-1} d$ for the corresponding constants of each phase. To capture the strong dependence of piezoelectric polarization coefficients of PMN-PT matrix on its texture due to the high anisotropy of PMN-PT single crystal, we use $b^M = b^{MR} + f(V_T)(b^{MT} - b^{MR})$, where $f(V_T) = 1 - \exp(-V_T/V_0)$ is a texture parameter function fitted to the Lotgering factor plotted in Fig. 1(b), with fitting parameter $V_0 = 0.003$. The theoretically predicted dielectric and piezoelectric properties of textured PMN-PT ceramics are plotted as a function of BT template volume fraction in Fig. 4, exhibiting good agreement with the experimental measurements shown in Figs. 2(a) and 2(b), especially for the piezoelectric strain coefficients d_{33} and d_{31}. These results confirm that [001] texturing of PMN-PT significantly improves the ceramic properties, while BT template content decreases the composite properties through mechanical clamping effect and interfacial mismatch.

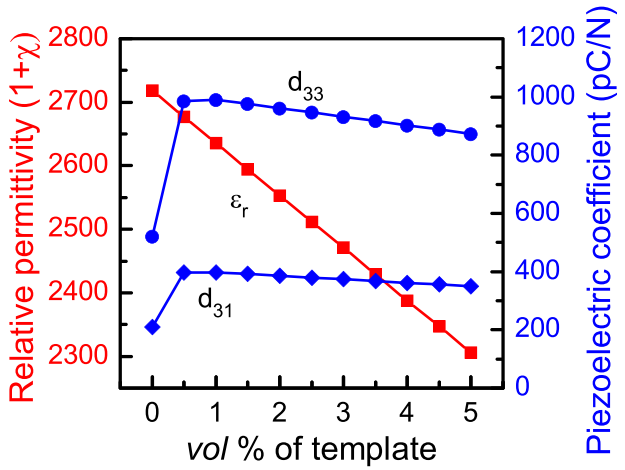

FIG. 4. Theoretical prediction of dielectric and piezoelectric properties of textured PMN-PT ceramics as a function of BT template volume fraction.

In conclusion, we quantify the effect of BT template heterogeneity on the texture degree and piezoelectric properties of PMN-PT ceramics. Inhomogeneity effect (elastoelectric composite effect, clamping strain) was clarified by theoretical models. Almost full [001] texture ($f = 0.98$) was achieved at very low template volume fraction (1%). This is an important advancement in texture engineering of PMN-PT ceramics that promises to provide high-performance piezoelectric materials at significantly lower cost.

Y. Yan and S. Priya gratefully acknowledge the financial support from DARPA (Synthesis) and Office of Basic Energy Science (DE-FG02-07ER46480). Y. U. Wang acknowledges support from DOE under Award No. DE-FG02-09ER46674.

[1]S. E. Park and T. R. Shrout, J. Appl. Phys. **82**, 1804 (1997).
[2]E. M. Sabolsky, S. Trolier-McKinstry, and G. L. Messing, J. Appl. Phys. **93**, 4072 (2003).
[3]S. Kwon, E. M. Sabolsky, G. L. Messing, and S. Trolier-McKinstry, J. Am. Ceram. Soc. **88**, 312 (2005).
[4]Y. K. Yan, H. P. Zhou, W. Zhao, and D. Liu, J. Electroceram. **21**, 246 (2008).
[5]Y. Saito, H. Takao, T. Tani, T. Nonoyama, K. Takatori, T. Homma, T. Nagaya, and M. Nakamura, Nature **432**, 84 (2004).
[6]Y. K. Yan, K. H. Cho, and S. Priya, J. Am. Ceram. Soc. **94**, 1784 (2011).
[7]E. M. Sabolsky, A. R. James, S. Kwon, S. Trolier-McKinstry, and G. L. Messing, Appl. Phys. Lett. **78**, 2551 (2001).
[8]G. L. Messing, S. Trolier-McKinstry, E. M. Sabolsky, C. Duran, S. Kwon, B. Brahmaroutu, P. Park, H. Yilmaz, P. W. Rehrig, K. B. Eitel, E. Suvaci, M. Seabaugh, and K. S. Oh, Crit. Rev. Solid State Mater. Sci. **29**, 45 (2004).
[9]T. Richter, S. Denneler, C. Schuh, E. Suvaci, and R. Moos, J. Am. Ceram. Soc. **91**, 929 (2008).
[10]F. K. Lotgering, J. Inorg. Nucl. Chem. **9**, 113 (1959).
[11]M. Zgonik, P. Bernasconi, M. Duelli, R. Schlesser, P. Gunter, M. H. Garrett, D. Rytz, Y. Zhu, and X. Wu, Phys. Rev. B **50**, 5941 (1994).
[12]Y. U. Wang, Appl. Phys. Lett. **96**, 232901 (2010).
[13]Y. U. Wang, J. Mater. Sci. **44**, 5225 (2009).
[14]A. G. Khachaturyan, *Theory of Structural Transformations in Solids* (Wiley, New York, 1983).
[15]S. P. Timoshenko and J. N. Goodier, *Theory of Elasticity*, 3rd ed. (McGraw-Hill, New York, 1969).
[16]Z. Y. Feng, X. Y. Zhao, and H. S. Luo, J. Phys. Condens. Matter **16**, 6771 (2004).